PNAS
www.pnas.org

Supplementary Information for

Molecular characterization of a fungal gasdermin-like protein

Asen Daskalov[a,e], Patrick S. Mitchell[c], Andrew Sandstrom[c], Russell E. Vance[c,d] and N. Louise Glass[a,b]

[a]Plant and Microbial Biology Department, The University of California, Berkeley, CA 94720
[b]Environmental Genomics and Systems Biology Division, The Lawrence Berkeley National Laboratory, 1 Cyclotron Road, Berkeley, CA 94720
[c]Division of Immunology and Pathogenesis, Department of Molecular and Cell Biology, University of California, Berkeley, CA 94720 USA
[d]Howard Hughes Medical Institute, University of California, Berkeley, CA 94720 USA
[e]Current address: CNRS, UMR 5248, European Institute of Chemistry and Biology, University of Bordeaux, Pessac, France

Corresponding authors

N. Louise Glass
The Plant and Microbial Biology Department
The University of California, Berkeley, CA 94720
510.643.2546
Lglass@berkeley.edu

Asen Daskalov
CNRS, UMR 5248, European Institute of Chemistry and Biology, University of Bordeaux, Pessac, France
asen.daskalov@u-bordeaux.fr

This PDF file includes:

Supplementary Materials and Methods
Tables S1, S2 and S3
Figures S1 to S8
SI References

Supplementary Materials and Methods

Plasmids, strains and media

N. crassa strains were grown using standard procedures and protocols that can be found on the Neurospora homepage at FGSC (www.fgsc.net/Neurospora/NeurosporaProtocolGuide.htm). Vogel's minimal media (VMM) was used to culture all strains, except when specified otherwise (1). Crosses were performed on Westergaard's synthetic cross medium (2). For flow cytometry experiments, thermo-reversible solid Vogel's media was obtained substituting the agar with 20% Pluronic F-127 (Sigma). The *Δrcd-1* (ΔNCU05712) deletion strain was obtained from the single gene deletion collection of *N. crassa* strains at the FGSC (3). All molecular constructs were introduced in the *his-3* locus of a *Δrcd-1* strain using standard transformation protocols. Molecular constructs were cloned in a pMF272-derived vector and expression was regulated by the constitutive *tef-1* promoter (4). The *rcd-1-2* allele was cloned downstream of the GFP with *Xba*I/*Pac*I restriction enzymes, while other fluorescently labeled *rcd-1* fusions have been described previously (5). The V5-*rcd-1-1* sequence was cloned under the *tef-1* promoter with *Bam*HI/*Pac*I restriction sites. Site-directed mutagenesis was performed with QuikChange II kit (Agilent), using manufacturer recommended procedures. For heterologous protein expression of RCD-1-1 and RCD-1-2 in insect cells (Sf9), we cloned codon-optimized 6xHis-tagged *rcd-1-1* and *rcd-1-2* sequences into a pAcSG2-derived vector using *Xho*I/*Not*I restriction enzymes.

For expression in human 293T kidney cells, codon-optimized *rcd-1-1* and *rcd-1-2* constructs were cloned in pcDNA3.1-derived vector under the control of constitutive CMV (cytomegalovirus) promoter using *Xho*I/*Not*I restriction sites to produce the PSM371 and PSM372 vectors, respectively. The two *rcd-1* alleles were cloned downstream of epitope tags 3xFLAG or HA and upstream of an internal ribosomal entry site (IRES), which controls the expression of fluorescence-emitting proteins (eGFP or mCherry).

Flow cytometry

Flow cytometry was performed according to (6). In brief, 90 µl sterile H_2O, containing conidia (3 x 10^7), were spread on plates (5 cm of diameter) containing 4 ml of Vogel's minimal media with 20% Pluronic F-127 (Sigma–Aldrich) instead of agar. Conidia were left germinating at 30° C in the dark for ~ 4 hrs. The plates were then placed at -20°C for 10 min to liquefy the Pluronic-containing media. Germlings are harvested by centrifugation (5 min at 2800 rpm) and washed twice with 1 ml of cold PBS. Washed germlings were suspended in 1 ml PBS in presence of 0.1 µM SYTOX Blue (Life Technologies) or 0.15 µM

propidium iodide (Sigma–Aldrich). Flow cytometry analyses were performed on a BD LSR Fortessa X-20 (BD Biosciences). SYTOX Blue vital dye was detected with a no dichroic 450/50 filter after excitation using a 405-nm laser. Fluorescence emitted by propidium iodide was detected with a 685 LP 710/50 filter after excitation with 488-nm laser. We recorded 20,000 events per sample for each experiment. Experiments were performed at least three times. Data was analyzed with custom MATLAB (MathWorks) script and ungerminated conidia were excluded from the analyses as previously described (6, 7). Cell death is shown as the average percentage of fluorescent events from all experiments.

Sucrose gradient centrifugation

Sucrose gradient cell fractionation protocols were similar to previously described methods (8). In brief, strains were grown on solid media for 7-10 days. Conidia were harvested, washed with Mili-Q water and inoculated at 10^6 conidia/ml in 100 ml of Vogel's media in a 250 ml flask. Flasks were incubated at 30˚C with constant shaking for 2.5 hours, followed by 2.5 hours at 30˚C without shaking, as to allow germling fusion. Germinated conidia were harvested by vacuum filtration and frozen in liquid nitrogen. Cells were lysed in 500 µl of STE10 (10% sucrose (w/w), 10 mM TrisHCl pH 7.5, 10 mM EDTA). Un-lysed cells were removed by centrifugation (5min, 5000 g at 4˚C) and 300 µl of the cleared lysate was loaded on top of 5 ml 20-60% (w/w) stacked sucrose gradient. Samples were ultracentrifuged (100 000 g) for 18 hours at 4˚C and 10 fractions of 500 µl were collected. Sample fractions were loaded on a 4-12% Bis-Tris NuPAGE gel, blotted on a PVDF membrane and probed with α-PMA-1 (ab4645), α-GFP (Roche) and α-V5 (Invitrogen R96025) antibodies.

Protein expression and purification

To produce recombinant RCD-1, the pAc-6xHisRCD-1-1, pAc-6xHisRCD-1-2 or pAc-6xHisV5-RCD-1-1, were co-transfected with BestBac linearized baculovirus DNA (Expression Systems) into Sf9 insect cells, following the manufacturer's protocol. Primary virus amplification and protein production were performed in Sf9 cells. In brief, RCD-1 was produced by infecting 2L of Sf9 cells (density of $1.5x10^6$) with one ml of amplified virus per liter of cells. Protein expression was carried at 28˚C for 64 hrs and cells were harvested by centrifugation at 300xg for 15 min. Cell pellets were resuspended in lysis buffer (50 mM Tris pH 7.4, 150 mM NaCl, 20 mM imidazole) and lysed on ice using a Dounce homogenizer (50 extrusions per sample). Samples were clarified at 20,000xg for 30 min and supernatants were batch bound to 1 ml of Ni-NTA agarose beads (Qiagen) for 2-3 hours at 4˚C. Protein purification was realized by gravity flow through on an Econo-Pac® chromatography column (Bio-Rad). Resin was washed with 100 ml of wash buffer (50 mM Tris pH 7.4, 400 mM NaCl, 20 mM imidazole) and 5 fractions of 1 ml were eluted with elution buffer (50 mM Tris pH 7.4, 150 mM NaCl, 250 mM imidazole). Fractions rich on protein were pooled (3 ml total) and desalted with an Econo-Pac® 10DG desalting prepacked gravity flow columns with TBS buffer (25 mM Tris pH 7.5, 150 NaCl, 3 mM KCl). Size-exclusion chromatography on a SEC 650 column (Bio-Rad) was performed as to further purify recombinant RCD-1.

Liposome preparation and binding assays

Unilamellar liposomes were produced based on the dry lipid film method as described in Liu *et al.* (9). For the liposome-binding essay, we produced liposomes with various proportions of synthetic 1-palmitoyl-2-oleoyl-sn-glycero-3-phosphocholine (POPC), 1,2-dioleoyl-sn-glycero-3-phosphoethanolamine (DOPE), 1,2-dioleoyl-sn-glycero-3-(phospho-L-serine) (DOPS), 1',3'-bis[1,2-dioleoyl-sn-glycero-3-phospho]-glycerol (cardiolipin; CL) (Avanti Polar Lipids). Liposomes used in EM experiments were composed of 1,2-Dipalmitoyl-sn-glycero-3-phosphoserine (DPPS), 1,2-Dipalmitoyl-sn-glycero-3-phosphoethanolamine (DPPE), 1,2-Dipalmitoyl-sn-glycero-3-phosphocholine (DPPC) and cardiolipin (CL) in ratio of 4:1:4:1. Lipids were dissolved in chloroform and mixed in a glass dram vial and the solvent was evaporated under permanent stream of N_2 gas. The dried lipid film was then hydrated with TBS (25 mM Tris pH 7.5, 150 NaCl, 3 mM KCl). The lipid suspensions were freeze-thawed in liquid nitrogen three times and vortexed during 5 min. Unilamellar liposomes were obtained with a mini-extruder device (Avanti Polar Lipids), 40 extrusion-passes, using membranes with 200 nm pores.

Recombinant RCD-1 was spun down for 30 min at 20,000xg, 4˚C, to ensure no large oligomers (particles) remain in suspension, and 5 µM of the protein were incubated with the indicated liposomes (500 µM lipids) for 30 min at RT, in a total volume of 80 µl. Samples were centrifuged at 24,000xg for 20 min at 4˚C and the supernatant (S) was separated from the pellet (P). The pellet was resuspended in the same volume as the supernatant (80 µl) and samples were loaded on a NuPAGE™ Novex 4-12% Bis-Tris protein gel for SDS-PAGE.

Table S1: Fungal RCD-1 homologs scored with HHPRED

ID	Species[1]	% Identity with RCD-1-1	mGSDMD (PDB: 6N9N), % Prob	mGSDMA3 (PDB: 6CB8), % Prob
RCD-1-1	***Neurospora crassa***	**-**	**94**	**87**
RCD-1-2	***Neurospora crassa***	**39%**	**93**	**89**
314724 (JGI prot ID)	*Neurospora hispaniola*	37%	94	92
512864 (JGI prot ID)	*Gelasinospora tetrasperma*	41%	94	92
XP_003350360	*Sordaria macrospora*	63%	90	72
XP_011127315	*Arthrobotrys oligospora*	44%	93	86
XP_013940825	*Trichoderma atroviride*	39%	92	81
XP_024727955	*Meliniomyces bicolor*	37%	92	89
XP_018158069	*Colletotrichum higginsianum*	35%	89	85
PNP43615	*Trichoderma gamsii*	34%	91	81
PHH79272	*Ophiocordyceps camponoti-rufipedis*	32%	86	73
XP_003046129	*Nectria haematococca*	30%	93	84
RWA10980	*Xylaria grammica*	32%	92	86
KJZ73710	*Hirsutella minnesotensis*	28%	92	92
PKK52750	*Trichoderma harzianum*	26%	94	90
XP_009222692	*Gaeumannomyces tritici*	32%	93	82
CEJ85931	*Torrubiella hemipterigena*	27%	94	91
EWZ32234	*Fusarium oxysporum*	30%	91	77
RYN30759	*Alternaria tenuissima*	26%	93	85
RFN43277	*Fusarium sp. FIESC_12*	24%	93	90
EMR62403	*Eutypa lata*	28%	93	88
OIW32351	*Coniochaeta ligniaria*	31%	95	91
EWC48475	*Drechslerella stenobrocha*	31%	92	84
KXX82511	*Madurella mycetomatis*	41%	95	87

[1] Select *rcd-1* homologs from the large family of homologs (>940) identified in filamentous fungi (5).

Table S2. Bacterial proteins related to gasderim and fungal RCD-1, scored with HHpred

Uniprot ID	Species[1]	GSDMD (PDB: 6N9N) % Probability	GSDMA3 (PDB: 6CB8) % Probability
A0A0S2DNG5	*Lysobacter enzymogenes*	99.03	99.32
A0A2T5RB28	*Geobacter sp. DSM 2909*	98.02	98.26
A0A2T4VDM4	*Vitiosangium sp. GDMCC 1.1324*	99.03	99.26
A4YML8	*Bradyrhizobium sp.*	99.2	99.41
A9WH26	*Chloroflexus aurantiacus*	99.54	99.65
A0A162CPX3	*Aquimarina aggregata*	98.78	98.99
I0H899	*Actinoplanes missouriensis*	98.21	98.36
A0A3G3GXX0	*Runella sp. SP2*	95.58	96.71
A0A1A5S462	*Mesorhizobium sp. AA22*	97.98	98.38

[1] Select *rcd-1* homologs from bacterial homologs (>940) identified in Daskalov *et al.,* (5).

Table S3. Strains used in this study.

Strain Name	Strain ID	Genotype	Source
rcd-1-1 (*NCU05712*)	AD57#17	*his-3::wtp-rcd-1-1 ΔNCU05712::hyg^R mat a*	This study
rcd-1-2	AD50#15	*his-3::wtp-rcd-1-2 ΔNCU05712:: hyg^R mat a*	This study
GFP	AD98#03	*his-3::ptef-GFP ΔNCU05712:: hyg^R mat a*	This study
GFP *rcd-1-1*	AD100#04	*his3::tefGFP mat a*	This study
GFP-RCD-1-1	AD90#10	*his-3::ptef-GFP-rcd-1-1 ΔNCU05712:: hyg^R*	This study
GFP-RCD-1-2	AD62#05	*his-3::ptef-GFP-rcd-1-2 ΔNCU05712:: hyg^R*	This study
mCh-RCD-1-2	AD133#mk5	*his-3::ptef-mCherry-rcd-1-2 ΔNCU05712:: hyg^R mat a*	This study
V5-RCD-1-1	AD103#10	*his-3::ptef-V5-rcd-1-1 ΔNCU05712:: hyg^R*	This study
R129	AD141#mk01	*his-3::ptef-GFP-rcd-1-1-R129A ΔNCU05712:: hyg^R mat a*	This study
K134	AD143#mk08	*his-3::ptef-GFP-rcd-1-1-K134A ΔNCU05712:: hyg^R mat a*	This study
K147	AD101#07	*his-3::ptef-GFP-rcd-1-1-K147A ΔNCU05712:: hyg^R*	This study
RK	AD145#mk15	*his-3::ptef-GFP-rcd-1-1-R129AK134A ΔNCU05712:: hyg^R mat a*	This study
KK	AD102#02	*his-3::ptef-GFP-rcd-1-1-K147AK149A ΔNCU05712:: hyg^R*	This study
KKK	AD115#mk3	*his-3::ptef-GFP-rcd-1-1-K134AK147AK149A ΔNCU05712:: hyg^R mat a*	This study
RKK	AD119#mk14	*his-3::ptef-GFP-rcd-1-1-R129AK147AK149A ΔNCU05712:: hyg^R mat a*	This study
RKKK	AD117#mk5	*his-3::ptef-GFP-rcd-1-1-R129AK134AK147AK149A ΔNCU05712:: hyg^R mat a*	This study
GFP-RCD-1-2-K146A	AD105#13	*his-3::ptef-GFP-rcd-1-2-K146A ΔNCU05712:: hyg^R*	This study
GFP-RCD-1-2-K146AK148A	AD107#11	*his-3::ptef-GFP-rcd-1-2-K146AK148A ΔNCU05712:: hyg^R*	This study

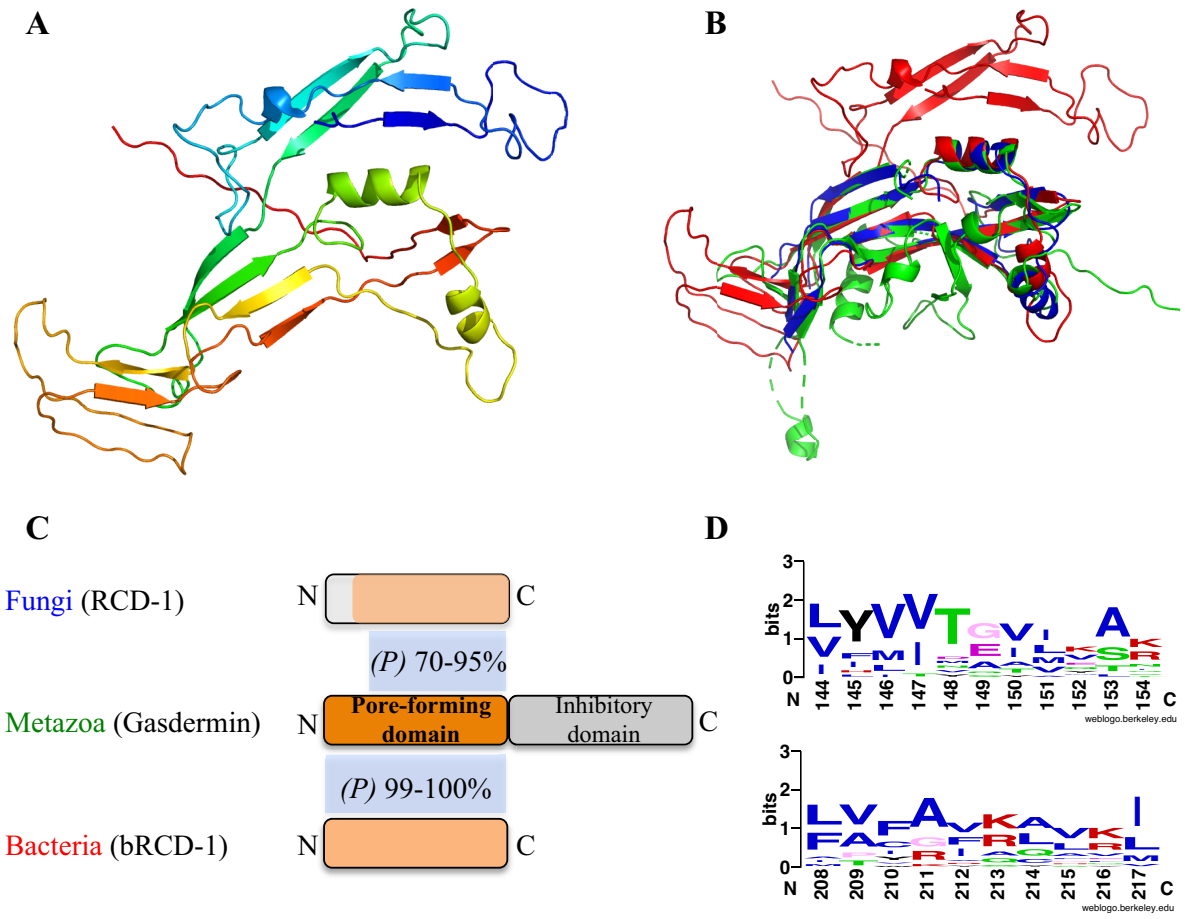

Figure S1. RCD-1/gasdermin proteins are found in Eukaryotes and Prokaryotes. (**A**) Homology modeling of RCD-1-1 with RaptorX (http://raptorx.uchicago.edu/). The molecular model was based on the structure of murine GSDMA3 (PDB – 5B5R), proposed as best template during the modeling process (p-value $2.02e^{-02}$). The model (side view) is shown in rainbow mode with residues from the N-terminal end towards the C-terminal end of the protein chain, colored in blue through the rainbow spectrum to red. (**B**) Structural alignment of murine GSDMD (6N9N) (blue), murine GSDMA3 (green) and the generated model of RCD-1-1 (red). Shown is a side view of the three overlaid structures. (**C**) Cartoon representation showing the homology between fungal RCD-1 proteins, metazoan gasdermins and the bacterial gasdermin-like proteins, some of which were previously identified in Daskalov *et al.*, (5). Probability scores of homology as obtained by HHPRED are shown between putatively homologous domains. (**D**) MEME motifs showing the consensus sequences for two highly conserved regions common to eukaryotic and prokaryotic homologous sequences, which also correspond to the boxed in red regions from Figure 1. Residue numbers are shown in reference to RCD-1-1.

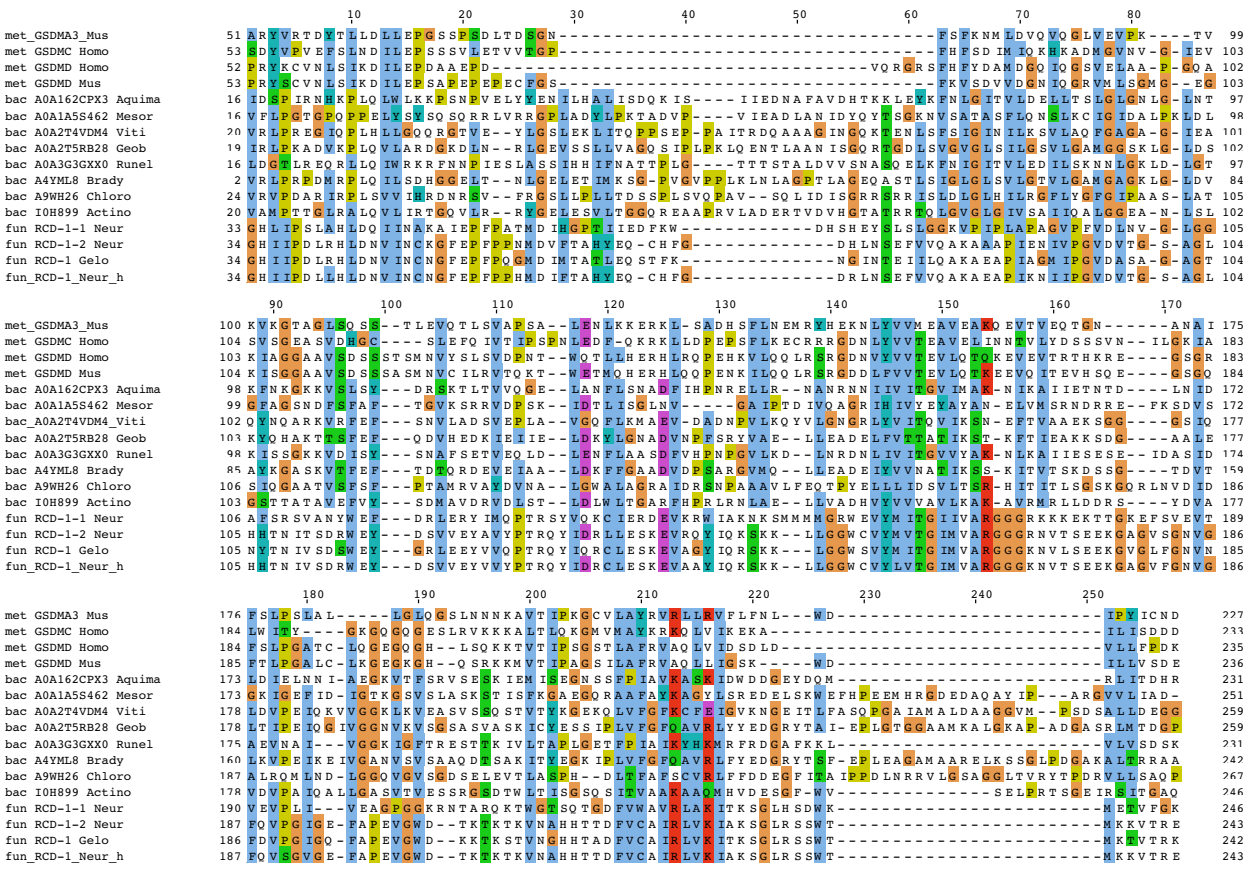

Figure S2. Protein alignment of RCD-1/GSDM sequences from Fungi (fun), Metazoa (met) and Bacteria (bac). Eight bacterial sequences are aligned with fungal and metazoan protein sequences used in the alignment in Figure 1. UniProt accession IDs are given for all eight bacterial sequences. Abbreviation of the species is as follows: Aquima - *Aquimarina aggregate,* Mesor - *Mesorhizobium sp. AA22*, Viti - *Vitiosangium sp. GDMCC 1.1324*, Geob - *Geobacter sp. DSM 2909,* Runel - *Runella sp. SP2,* Brady - *Bradyrhizobium sp.,* Chloro - *Chloroflexus aurantiacus,* Actino - *Actinoplanes missouriensis*. Conserved residues are shown in ClustalX colors, based on the nature of the amino acid residues: hydrophobic – blue, polar – green, negative charge – magenta, positive charge – red, aromatic – cyan, glycine – orange, proline – yellow, cysteine – pink, any/gap – white.

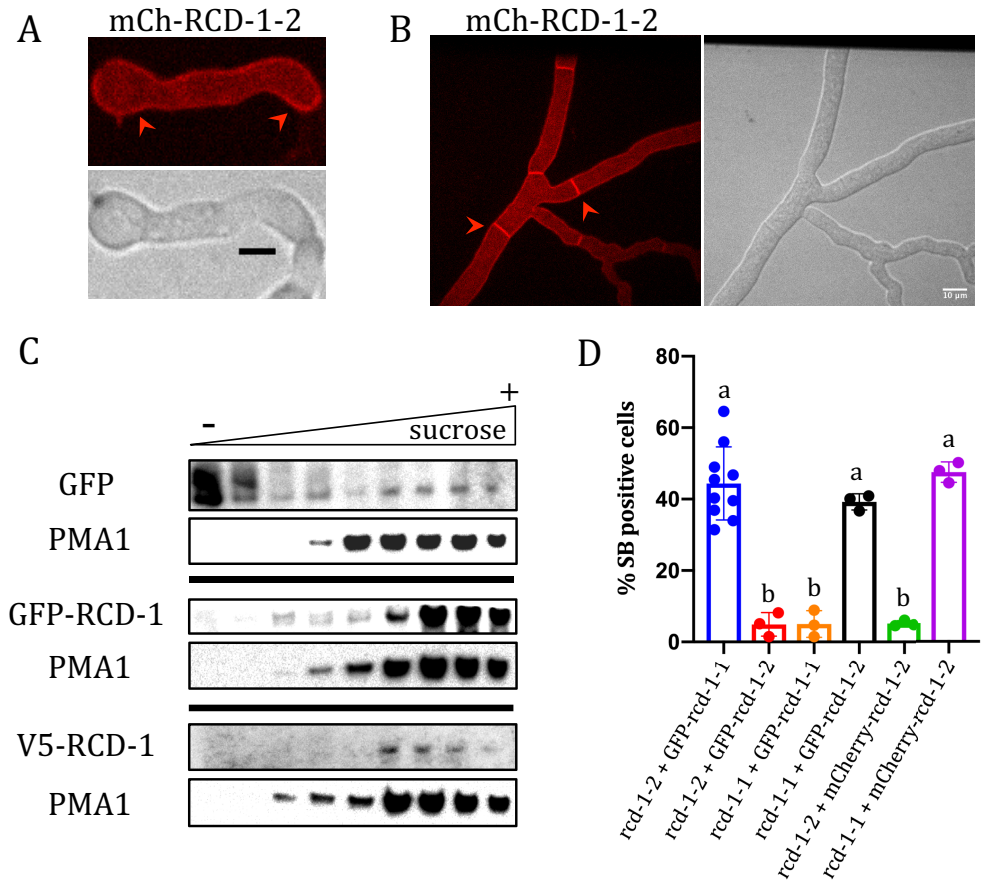

Figure S3. Plasma membrane and septal cellular localization for fluorescently labeled RCD-1. Fluorescent microscopy of mCherry-RCD-1-2 shows plasma membrane localization in germinating asexual spores of *N. crassa* (**A**) and in hyphae (**B**), where the protein equally localizes to the septa (red arrowheads). Scale bars are 5 µm and 10 µm. (**C**) Sucrose density gradient (10-60%) ultracentrifugation experiment (8) with GFP-labeled or V5-labeled RCD-1-1. Cellular membranes were tracked by antibodies to PMA1 (plasma membrane ATPase 1)(10,11) and were found in the denser fractions, while free GFP control reveals fractions containing the cytoplasmic content. (**D**) Flow cytometry quantification of the cell death-inducing competency of GFP-RCD-1-1 and GFP-RCD-1-2. Cell death is measured as proxy by quantifying the SYTOX Blue (vital dye) positive population of paired germlings after 4 hrs of growth. Germlings that undergo cell fusion and that express functional antagonistic *rcd-1* alleles (*rcd-1-1* and *rcd-1-2*) undergo rapid cell death (5). Experiments were performed at least in triplicate, with 20,000 events counted per experiment. P value ($a \neq b$) < 0.0002, one-way ANOVA with Tukey's multiple comparisons test.

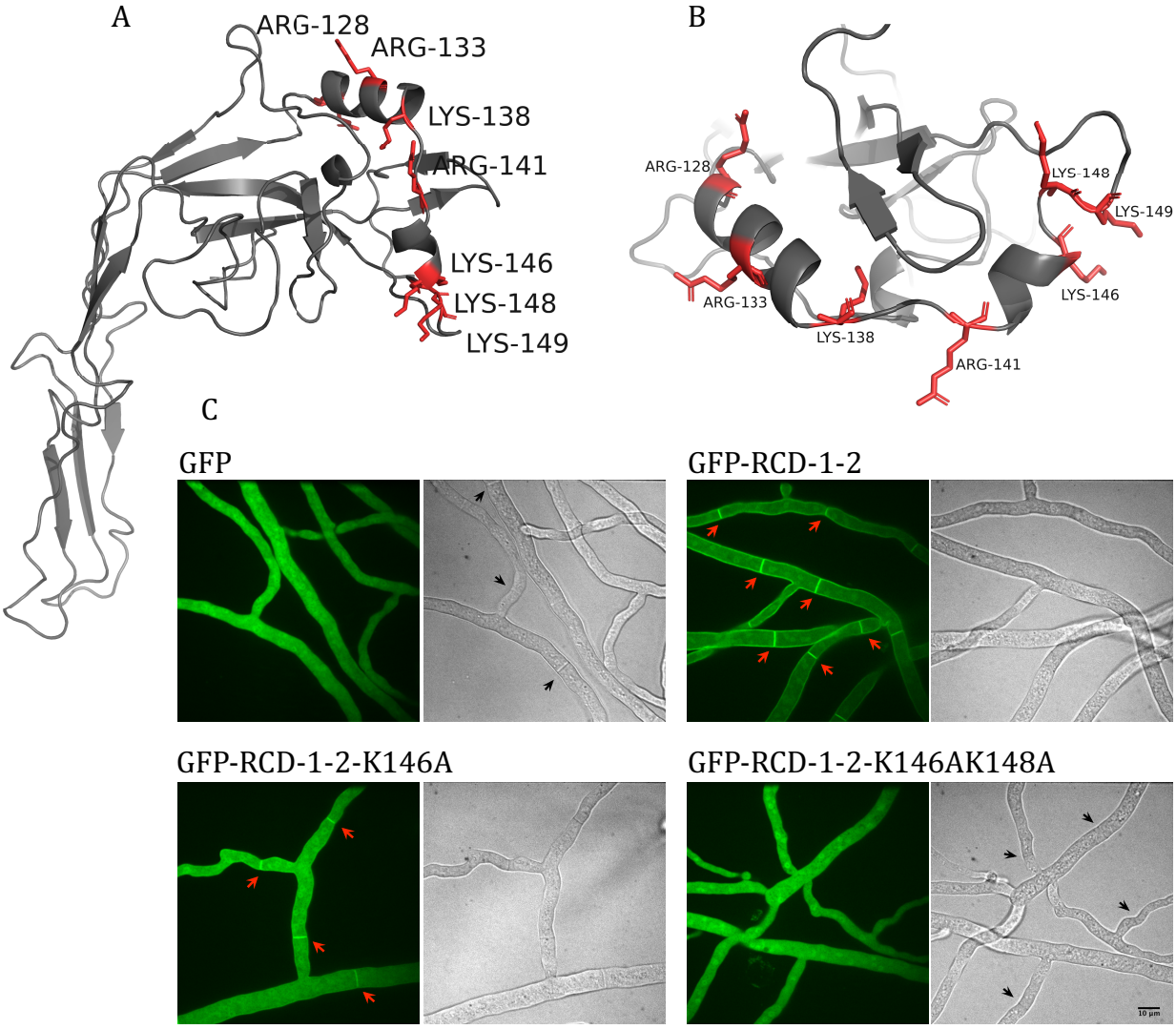

Figure S4. Cellular localization of RCD-1-2 is dependent on set of positively charged residues on a predicted pair of α-helices. (**A**) Molecular model of RCD-1-2 (side view), based on murine gasdermin A3 (6CB8). Positively charged amino acid residues (Lysine (K) and Arginine(R)) are highlighted in red. (**B**) Zoom-in of the helical region of the RCD-1-2 molecular model. Seven positively charged residues, decorating the solvent-exposed side of the pair of helices, are shown in red. (**C**) Fluorescence microscopy of GFP-RCD-1-2 and mutant GFP-RCD-1-2 proteins in hyphae. Red arrows show septal and membrane association of GFP-RCD-1-2. Black arrowheads point towards septa that do not show GFP-RCD-1-2$^{K146A;K148A}$ localization. Scale bar is 10 µm.

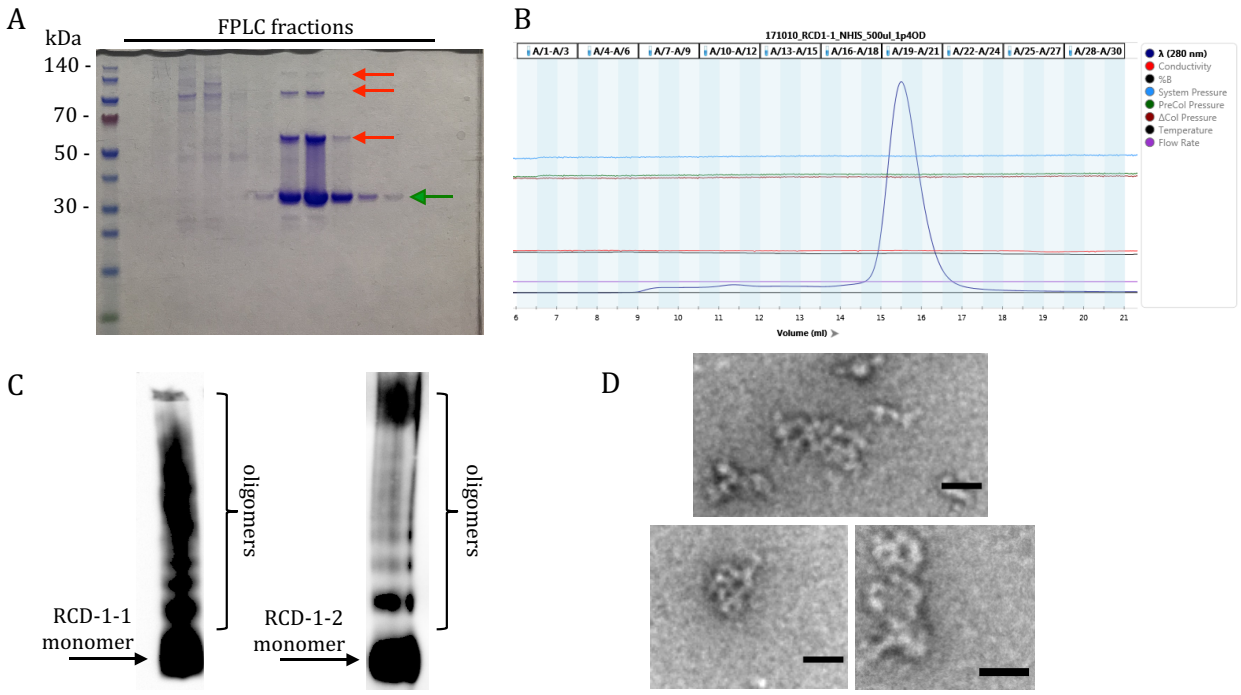

Figure S5. ***In vitro*** **characterization of RCD-1.** (**A**) Polyacrylamide gel electrophoresis (PAGE) and Coomassie blue-stained gel of FPLC (Fast protein liquid chromatography) fractions of Ni-affinity purified 6xHis-tagged RCD-1-1. The protein migrates at the expected for a monomer size of ~30 kDa (green arrow). Red arrows point to protein bands likely corresponding to RCD-1-1 SDS-resistant oligomers. Because the fractions in which these bands appear correspond to proteins with lower molecular weight, we concluded that the RCD-1-1 aggregates are formed *de novo* after the size-exclusion chromatography was performed. (**B**) Shown is SEC profile (size exclusion chromatography) for RCD-1-1 (both RCD-1-1 and RCD-1-2 showed virtually identical profiles) with the protein eluting predominantly as a monomer (fractions 19-21). The obtained SEC profile suggests that the RCD-1 oligomeric states are distributed in high number of fractions of higher molecular size. (**C**) Native-PAGE of RCD-1-1 and RCD-1-2 FPLC-purified protein samples. (**D**) Electron micrographs of protein aggregates formed by FPLC-purified RCD-1. Scale bars are 40 nm.

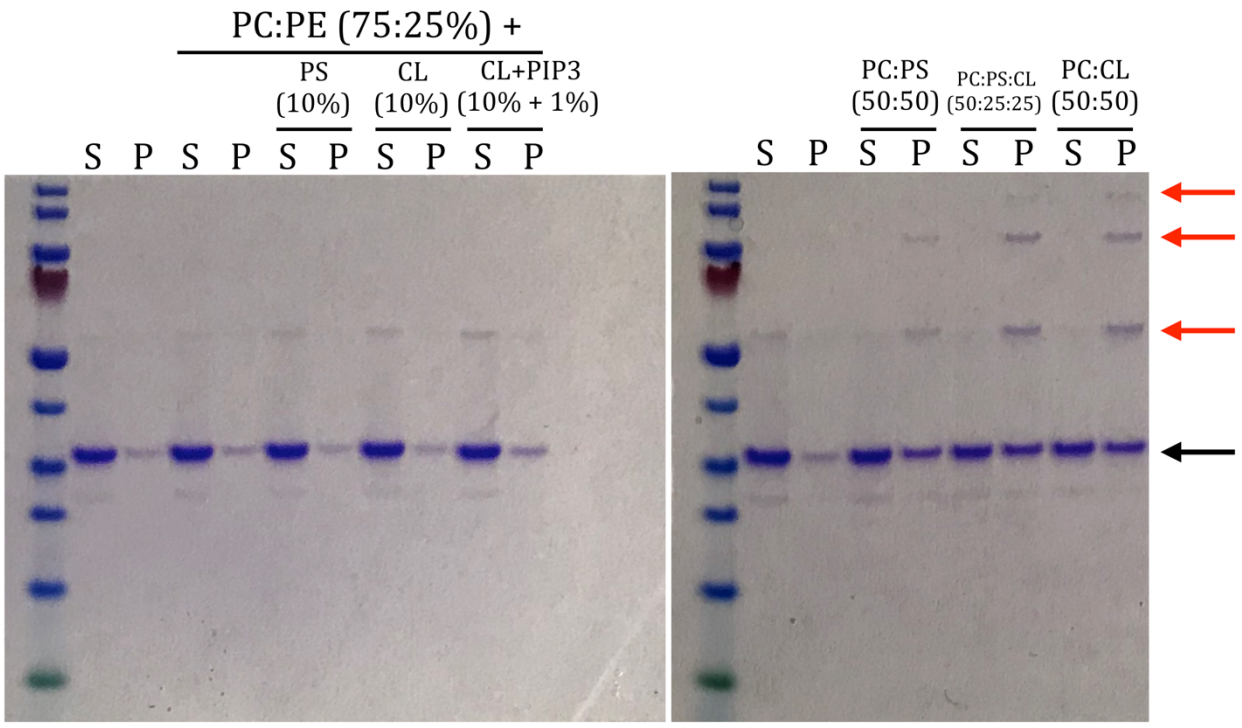

Figure S6. RCD-1-1 interacts with cardiolipin (CL) and phosphatidylserine (PS)-containing liposomes. Coomassie blue stained polyacrylamide gel with FPLC-purified RCD-1-1 alone or in presence of liposomes with various lipid compositions. After incubation with the liposomes, two fractions are obtained by centrifugation – a soluble fraction (S) and a pellet fraction (P) – which are loaded separately on the gel. Black arrow points to the protein band corresponding to monomeric RCD-1-1. Red arrows point to SDS-resistant dimers and likely other oligomeric forms of RCD-1-1. The protein remains in the soluble fractions after incubation with liposomes composed predominantly of phosphatidylethanolamine (PE) and phosphatidylcholine (PC) but is enriched in the pellet fraction when incubated with liposomes containing at least 25% of cardiolipin (CL) or phosphatidylserine (PS). Lipid composition of the liposomes for different samples is shown above the gels in percentage for each lipid.

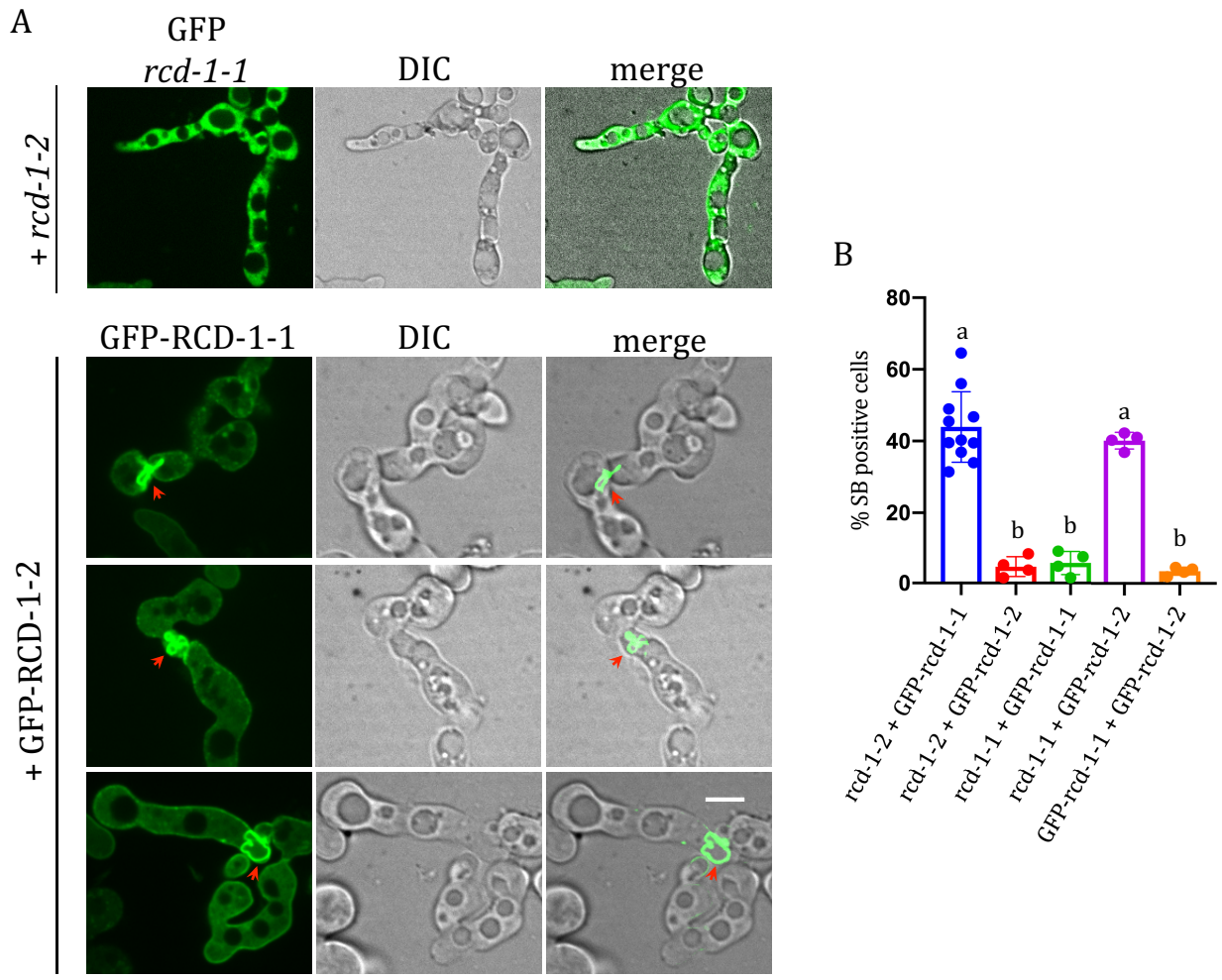

Figure S7. RCD-1 forms highly ordered molecular assemblies *in vivo*. (**A**) Upper panel shows fluorescent microscopy of fused germlings expressing incompatible RCD-1 variants and cytoplasmic GFP. Bottom panels show highly ordered (almost fibrillar) fluorescent assemblies (red arrowheads) in fused germlings bearing GFP-RCD-1-1 and GFP-RCD-1-2 and which are strongly vacuolated. Scale bar is 5 µm. (**B**) Flow cytometry quantification of the cell death-inducing competency of paired germlings bearing GFP-RCD-1-1 and GFP-RCD-1-2 as compared to controls. Cell death is measured by the uptake of the vital dye SYTOX blue (SB). Experiments were performed at least in triplicate, with 20,000 events counted per experiment. P value (a ≠ b) < 0.0001, one-way ANOVA with Tukey's multiple comparisons test.

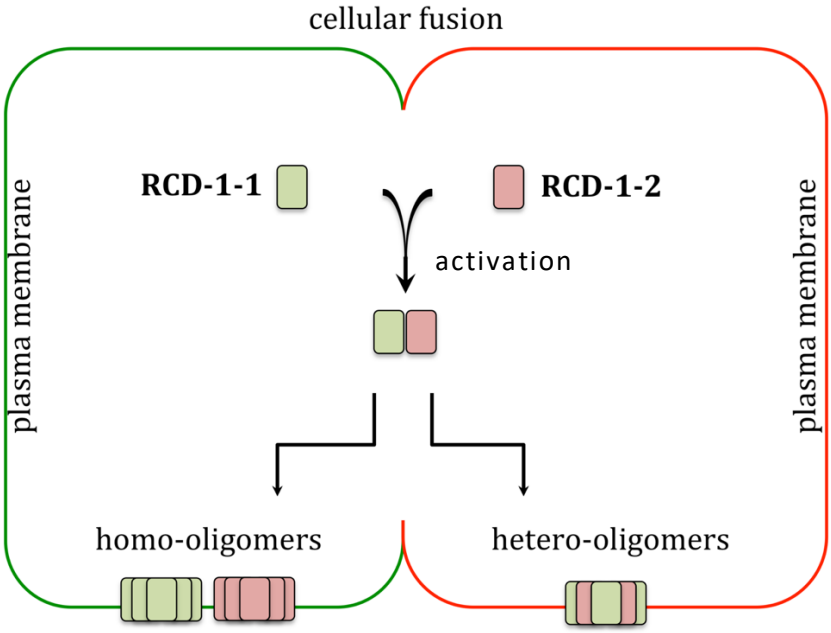

Fig. S8. Model of RCD-1-1/RCD-1-2 cell death mechanisms. Direct interaction of RCD-1-1 with RCD-1-2 after cellular fusion leads to the formation of RCD-1 aggregates, which induces membrane damage and trigger programmed cell death. Two possible molecular models are proposed. In the first (on the left), after activation via interactions between antagonistic RCD-1 proteins (RCD-1-1 + RCD-1-2), each RCD-1 variant oligomerizes in a homotypic manner to form a pore or a pore-like structure, while in the second model (on the right), following cell fusion, the two variants form hetero-oligomers, which carries the cytotoxic activity. While the activation step – the interaction between RCD-1-1 and RCD-1-2 – is common to both models, some experimental data, notably the ability of each RCD-1 allelic variant to self-oligomerize *in vitro*, suggests that homo-oligomers (like gasdermin) are the main carrier of the cytotoxic activity *in vivo* and thus the likeliest of the two models.

References

1. Vogel HJ (1956) A convenient growth medium for *Neurospora crassa*.
2. Westergaard M, Mitchell HK (1947) Neurospora V. A synthetic medium favoring sexual reproduction. *Am J Bot* 34(10):573–577.
3. Colot HV, et al. (2006) A high-throughput gene knockout procedure for *Neurospora* reveals functions for multiple transcription factors. *Proc Natl Acad Sci USA* 103(27):10352–10357.
4. Freitag M, Hickey PC, Raju NB, Selker EU, Read ND (2004) GFP as a tool to analyze the organization, dynamics and function of nuclei and microtubules in *Neurospora crassa*. *Fungal Genet Biol* 41(10):897–910.
5. Daskalov A, Gladieux P, Heller J, Glass NL (2019) Programmed cell death in *Neurospora crassa* is controlled by the allorecognition determinant *rcd-1*. *Genetics* 213(4):1387–1400.
6. Heller J, Clavé C, Gladieux P, Saupe SJ, Glass NL (2018) NLR surveillance of essential SEC-9 SNARE proteins induces programmed cell death upon allorecognition in filamentous fungi. *Proc Natl Acad Sci USA* 115(10):E2292–E2301.
7. Gonçalves AP, et al. (2019) Allorecognition upon fungal cell-cell contact determines social cooperation and impacts the acquisition of multicellularity. *Curr Biol*. 29(18):3006-3017
8. Fischer MS, Jonkers W, Glass NL (2019) Integration of self and non-self recognition modulates asexual cell-to-cell communication in *Neurospora crassa*. *Genetics* 211(4):1255–1267.
9. Liu X, et al. (2016) Inflammasome-activated gasdermin D causes pyroptosis by forming membrane pores. *Nature* 535(7610):153–158.
10. Bowman BJ, Blasco F, Slayman CW (1981) Purification and characterization of the plasma membrane ATPase of *Neurospora crassa*. *J Biol Chem* 256(23):12343–12349.
11. Bowman BJ, Borgeson CE, Bowman EJ (1987) Composition of *Neurospora crassa* vacuolar membranes and comparison to endoplasmic reticulum, plasma membranes, and mitochondrial membranes. *Exp Mycol* 11(3):197–205.